THE JOURNAL OF BIOLOGICAL CHEMISTRY VOL. 291, NO. 52, pp. 26899–26912, December 23, 2016

The N-terminal Ankyrin Repeat Domain Is Not Required for Electrophile and Heat Activation of the Purified Mosquito TRPA1 Receptor*

Received for publication, June 15, 2016, and in revised form, November 1, 2016 Published, JBC Papers in Press, November 14, 2016, DOI 10.1074/jbc.M116.743443

Sabeen Survery[‡], **Lavanya Moparthi**[‡], **Per Kjellbom**[‡], **Edward D. Högestätt**[§], **Peter M. Zygmunt**[§1], and **Urban Johanson**[‡2]

From the [‡]*Department of Biochemistry and Structural Biology, Center for Molecular Protein Science, Lund University, SE-221 00 Lund, Sweden and the* [§]*Clinical Chemistry and Pharmacology, Department of Laboratory Medicine, Lund University, SE-221 85 Lund, Sweden*

Edited by F. Anne Stephenson

Temperature sensors are crucial for animals to optimize living conditions. The temperature response of the ion channel transient receptor potential A1 (TRPA1) is intriguing; some orthologs have been reported to be activated by cold and others by heat, but the molecular mechanisms responsible for its activation remain elusive. Single-channel electrophysiological recordings of heterologously expressed and purified *Anopheles gambiae* TRPA1 (AgTRPA1), with and without the N-terminal ankyrin repeat domain, demonstrate that both proteins are functional because they responded to the electrophilic compounds allyl isothiocyanate and cinnamaldehyde as well as heat. The proteins' similar intrinsic fluorescence properties and corresponding quenching when activated by allyl isothiocyanate or heat suggest lipid bilayer-independent conformational changes outside the N-terminal domain. The results show that AgTRPA1 is an inherent thermo- and chemoreceptor, and analogous to what has been reported for the human TRPA1 ortholog, the N-terminal domain may tune the response but is not required for the activation by these stimuli.

The discovery of transient receptor potential (TRP)[3] ion channels, such as the TRP subtype A1 (TRPA1), being involved in chemo- and thermosensation, has opened up new avenues for understanding how organisms monitor the physicochemical environment (1–5). The identification by us and others of TRPA1 as a chemosensor activated by plant-derived electrophilic and thiol-reactive compounds (6–9), including isothiocyanates and diallyl disulfide from mustard and garlic, together with findings from numerous subsequent studies have established TRPA1 as a unique detector of tissue-damaging environmental chemicals and proinflammatory compounds in both invertebrates and vertebrates (5, 10–12).

Several TRPA1 homologues exist in the animal kingdom, and the ability of TRPA1 to sense potentially harmful electrophilic compounds has been conserved for ~500 million years, whereas the ancestral thermosensitive properties of TRPA1 are unclear and diverged later (5, 11). A role for mammalian TRPA1, and especially the human TRPA1 (hTRPA1), as noxious cold sensors has been controversial ever since it was proposed (13), whereas the heat-sensitive role of TRPA1 homologues in non-mammalians has been easily accepted (5, 10). However, we have recently shown that hTRPA1 is indeed an intrinsically cold-sensitive protein (14). If it is true that all TRPA1s are intrinsic thermo-gated ion channels, then it appears that human, rat, and mouse TRPA1 respond to cold temperatures below 20 °C, whereas, for example, the rattlesnake, fruit fly, and mosquito TRPA1 respond to warm temperatures above 25 °C (13, 15–24). However, this simplistic view may not hold true because it was recently shown that human TRPA1 also responds to heat (25).

It has been suggested that the intracellular N-terminal ankyrin repeat domain (ARD) of TRPA1 in snakes contains the necessary thermosensitive modules for heat detection, whereas both the N-terminal ARD and the pore region of *Drosophila* (*melanogaster*) TRPA1 may contain heat-sensitive elements (4, 16, 18, 26, 27). However, these and similar conclusions have to be regarded with some caution because the use of mutagenic and chimeric strategies results in artificial constructs, which makes it difficult to exclude indirect effects on a temperature sensor located elsewhere in the protein (5, 10). Furthermore, each of three single point mutations of amino acids in the N-terminal ARD, not previously regarded critical, like certain cysteine and lysine residues (28, 29), changed the mouse TRPA1 from being cold-sensitive to being heat-sensitive (30). Importantly, the authors concluded that this could best be explained by an effect on the coupling of temperature to channel gating rather than altering the nature of the thermosensitive domain itself (30). This reasoning is in line with our view that

* This work was supported by Vetenskapsrådet Grants 2014-3801, 2010-5787 (to P. M. Z. and E. D. H.), and 2007-6110 (to U. J.) and Svenska Forskningsrådet Formas Grant 2007-718 (to P. M. Z., E. D. H., U. J., and P. K.); the Research School of Pharmaceutical Sciences FLÄK (to U. J. and P. M. Z.); and the Medicinska Fakulteten, Lunds Universitet (to P. M. Z. and E. D. H.). The authors declare that they have no conflicts of interest with the contents of this article.

[1] To whom correspondence may be addressed. E-mail: peter.zygmunt@med.lu.se.

[2] To whom correspondence may be addressed. E-mail: urban.johanson@biochemistry.lu.se.

[3] The abbreviations used are: TRP, transient receptor potential; hTRPA1 and AgTRPA1, human and *Anopheles gambiae* TRPA1, respectively; ARD, ankyrin repeat domain; AITC, allyl isothiocyanate; SRCD, synchrotron radiation circular dichroism; G_s, single-channel conductance; Q_{10}, temperature coefficient; Ni-NTA, nickel-nitrilotriacetic acid; ITO, indium tin oxide; PDB, Protein Data Bank.

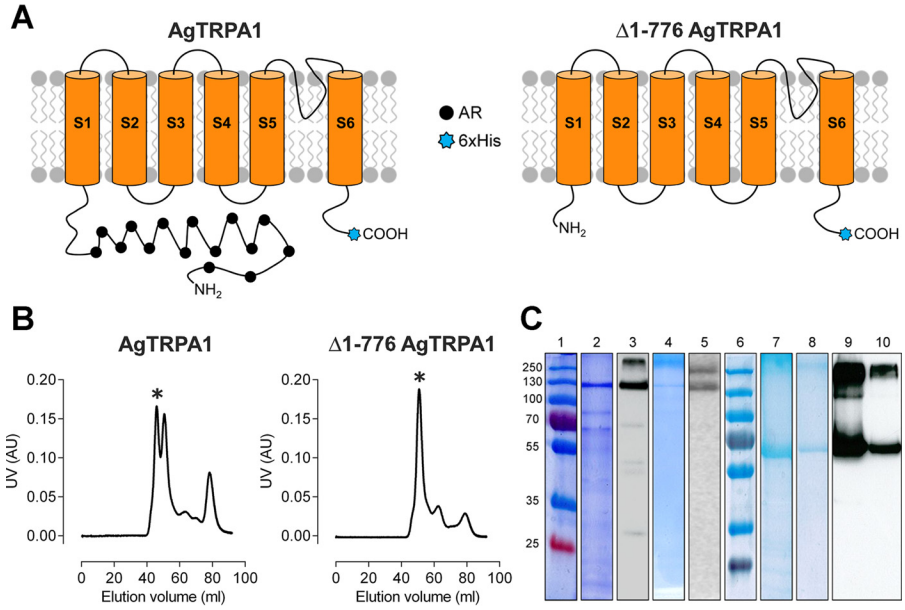

FIGURE 1. **Purification of full-length AgTRPA1 and N-terminally truncated (Δ1–776 AgTRPA1) constructs.** *A*, schematic representation of AgTRPA1 and Δ1–776 AgTRPA1 showing the N-terminal truncation, the six transmembrane helices (*S1–S6*) with the pore region connecting the last two helices (*S5* and *S6*), and the N and C termini facing the cytoplasm. The N-terminal containing ankyrin repeats (*AR*; *filled black circles*) and C-terminal hexa-His tag (*6xHis*; *blue stars*) are also indicated. *B*, purification profile of AgTRPA1 and Δ1–776 AgTRPA1 using a Superdex 200 16/26 column with the tetrameric fraction indicated by an *asterisk*. *C*, SDS-PAGE and Western blotting of AgTRPA1 and Δ1–776 AgTRPA1. The *panel* is assembled from several gels and blots; thus, two molecular mass markers are shown. *Lanes 1* and *6*, molecular mass markers (in kDa); *lanes 2* and *3*, AgTRPA1 after Ni-NTA affinity chromatography; *lanes 4* and *5*, tetrameric fraction after size exclusion chromatography. *Lanes 7* and *9*, Δ1–776 AgTRPA1 after Ni-NTA affinity chromatography; *lanes 8* and *10*, tetrameric fraction after size exclusion chromatography. Two major bands are seen in Western blots of the purified proteins (*lanes 5* and *10*) corresponding to monomeric and multimeric forms of the proteins.

conformational changes of the N-terminal ARD indirectly affect thermo- and chemosensitive structures outside the N-terminal ARD of TRPA1 (10, 14). Studies of purified TRPA1 without its N-terminal ARD should therefore be a valuable contribution in the search for TRPA1 thermo- and chemosensory domains (14). Clearly, various methodological approaches are needed to identify the location of distinct temperature-sensing domains if they exist at all (31–34).

The *Anopheles gambiae* TRPA1 (AgTRPA1), which exists as the two isoforms AgTRPA1(A) and AgTRPA1(B), is heat-sensitive as well as activated by electrophilic compounds when expressed heterologously (12, 16, 17, 23, 24). Depending on the anatomical location and isoform, AgTRPA1 is linked to avoidance or host-seeking behaviors (16, 23, 35). In the present study, we have purified the AgTRPA1(A) with the aim to determine whether this protein has inherent thermo- and chemosensitive properties and whether such properties are also located outside the N-terminal ARD. We show that AgTRPA1, irrespective of its N-terminal ARD, undergoes conformational changes and is activated by the electrophilic compounds allyl isothiocyanate (AITC) and cinnamaldehyde, as well as by temperatures above 25 °C. Thus, our recent proposal that electrophiles modify TRPA1 channel activity by interacting with binding sites, such as cysteine and lysine residues, outside the N-terminal ARD (14) is not restricted to hTRPA1 but also valid for the heat-sensitive AgTRPA1. Most important is our conclusion that temperature-sensitive regions of AgTRPA1 should be searched for outside the N-terminal ARD, as proposed for the cold-sensitive hTRPA1 (14).

Results

Overexpression and Purification of AgTRPA1—The methylotrophic yeast *Pichia pastoris* has been established as an excellent host for efficient expression of a number of heterologous eukaryotic membrane proteins (14, 36, 37). In this study, we have used this system to express the full-length isoform A of AgTRPA1 (16, 23) as well as a truncated construct lacking the N-terminal ARD (Δ1–776 AgTRPA1; Fig. 1*A*). After cell lysis, peripheral proteins were removed from the *Pichia* membrane fraction by urea and alkali washes, and TRPA1 proteins were extracted by the detergent fos-choline-12, which was identified as the best choice for protein stability and yield in screens performed with various detergents (data not shown). The proteins were further purified, by means of a hexa-His tag in the C-terminal extension by nickel affinity chromatography followed by size exclusion chromatography. The highly expressed Δ1–776 AgTRPA1 was quite pure already after the affinity purification, whereas the full-length construct suffered from both contaminating proteins and some degradation products after the corresponding step (Fig. 1*C*). In size exclusion chromatography, Δ1–776 AgTRPA1 eluted mainly as a tetramer, whereas AgTRPA1 eluted as a double peak corresponding to the tetramer and the dimer (Fig. 1*B*). After the two-step purification, the tetrameric Δ1–776 AgTRPA1 yield was estimated to be 1.3 mg from 20 g of *Pichia* cells. In comparison, the yield of the 2.5 times longer AgTRPA1 was found to be 0.7 mg from the same amount of cells. Only the tetrameric fractions were used for structural and functional characterization of TRPA1.

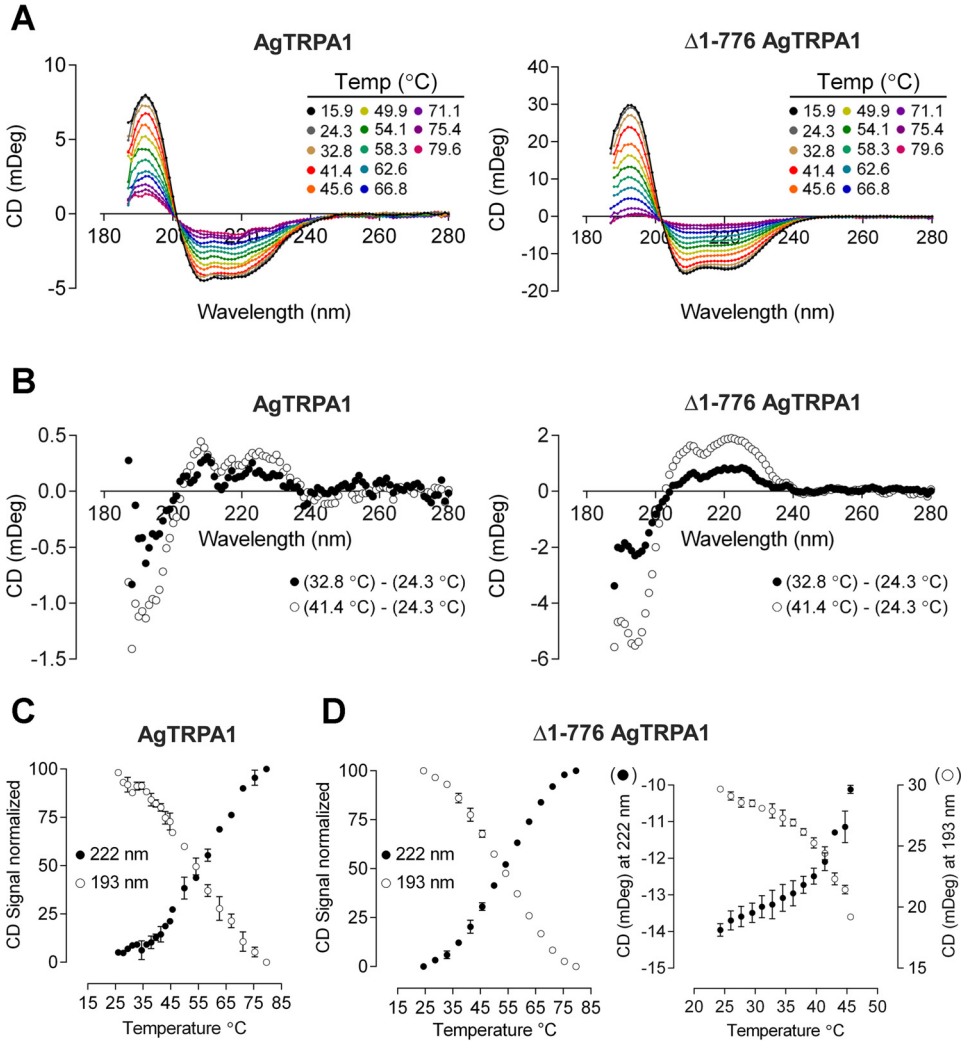

FIGURE 2. **SRCD spectra and thermal transition curves.** *A*, SRCD spectra of AgTRPA1 and Δ1–776 AgTRPA1 obtained at higher temperatures show gradual loss of the maximum at 193 nm and the two minima at 210 and 222 nm that are characteristic for α-helical proteins. *B*, differential plot of spectra recorded at two different temperatures for AgTRPA1 and Δ1–776 AgTRPA1. *C* and *D*, normalized transition curves at 193 and 222 nm as a function of temperature for AgTRPA1 (*C*; $n = 2$) and Δ1–776 AgTRPA1 (*D*; $n = 2$). Additional data points collected between 24 and 45 °C for the latter construct (*right*) are plotted without normalization of data ($n = 3$). In *C* and *D*, the average is plotted, and *error bars* indicate S.D.

Synchrotron Radiation Circular Dichroism Spectra and Thermal Denaturation of AgTRPA1—The tetrameric fractions of purified AgTRPA1 and Δ1–776 AgTRPA1 were subjected to synchrotron radiation circular dichroism (SRCD) spectroscopy to examine their overall fold and thermal unfolding (Fig. 2*A*). At low temperature, the SRCD spectra of both constructs exhibited the expected characteristic α-helical protein signature with a maximum at 193 nm and two deep minima at 210 and 222 nm, suggesting that the proteins retained their native fold after purification. The SRCD spectra obtained at higher temperatures show that both proteins gradually lose their secondary structure to become almost completely unfolded around 80 °C. The unfolding appears to be irreversible because lowering the temperature does not result in the reappearance of an α-helical spectrum (data not shown).

TRPA1 channels are believed to act as thermoreceptors; hence, we performed more careful analysis of the thermal denaturation of AgTRPA1 and Δ1–776 AgTRPA1 to monitor temperature-induced changes in the purified proteins. From differential plots of the spectra obtained at 24.3 °C and at 41.4 °C, the most prominent changes were found at 193 nm and at 222 nm (Fig. 2*B*). Therefore, we chose these two wavelengths for construction of thermal transition curves (Fig. 2, *C* and *D*). Although the complete transition of the truncated construct has a slightly lower midpoint (Table 1; ~54 °C, both at 193 and 222 nm) than the full-length TRPA1 (55 and 58 °C at 193 and 222 nm, respectively), there appear to be additional early minor transitions at 30 and 45 °C in the latter. A closer investigation of the thermal denaturation between 24 and 45 °C in the truncated construct cannot conclusively support or exclude a similar early transition at 30 °C due to the relatively large variability

TABLE 1

Midpoints of temperature transitions for AgTRPA1 and Δ1–776 AgTRPA1 as measured by SRCD

The midpoint ± S.D. was obtained from a fitted curve to two experiments.

AgTRPA1			Δ1–766 AgTRPA1		
Midpoint 193 nm	Midpoint 222 nm	*n*	Midpoint 193 nm	Midpoint 222 nm	*n*
°C	°C		°C	°C	
55.3 ± 0.8	58.1 ± 0.8	2	53.6 ± 1.0	53.8 ± 1.1	2

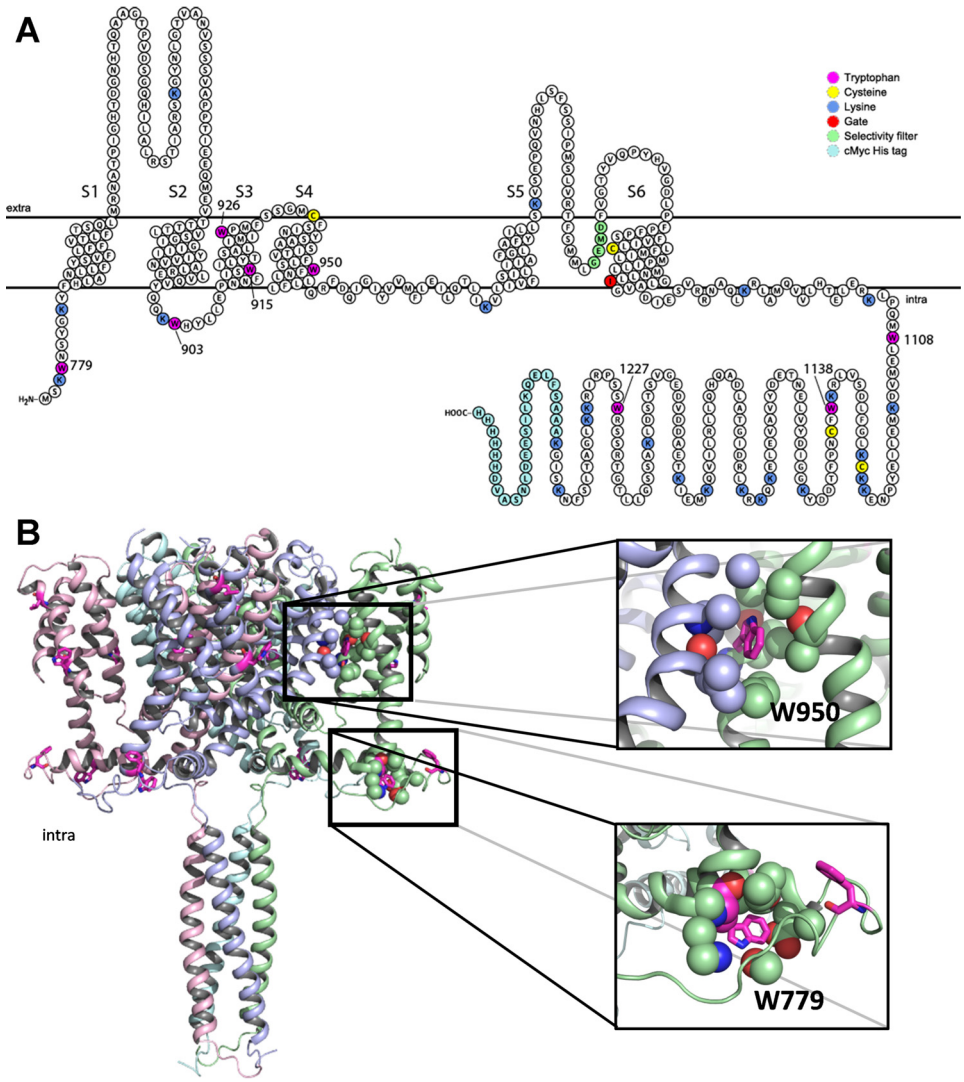

FIGURE 3. **Tryptophan positions and potential AITC binding sites.** *A*, topology plot of Δ1–776 AgTRPA1 highlighting all lysines and cysteines, which are potential binding sites for AITC, as well as the eight tryptophans. *B*, equivalent structure of tetrameric human TRPA1 (PDB entry 3J9P without the N-terminal ARD). The monomers are *color-coded*, and residues corresponding to tryptophans in Δ1–776 AgTRPA1 are indicated in *magenta*, omitting Trp-903, Trp-1138, and Trp-1227, which are located in unresolved regions. Transmembrane domains are shown at the *top*, and cytoplasmic regions are shown in the *bottom half* of the picture. *Close-ups* are shown of two conserved tryptophan residues, corresponding to Trp-779 and Trp-950 in AgTRPA1. A similar setting of these residues in AgTRPA1 and hTRPA1 is supported by the alignment in Fig. 4. Trp-950 in helix S4 is positioned in a hydrophobic pocket, sandwiched between helices S1 and S5 from a neighboring monomer, whereas Trp-779 resides in a more polar environment, likely to result in a lower quantum yield of fluorescence. All atoms within 5 Å of the indole ring of the tryptophans are shown as *spheres*; oxygen and nitrogen atoms are *colored red* and *dark blue*, respectively.

between samples, but a distinct transition between 41 and 43 °C is observed (Fig. 2*D*).

Intrinsic Tryptophan Fluorescence Is Quenched by an Agonist and Temperature—In contrast to CD spectrometry that monitors the secondary structure of a protein, tryptophan residues in a protein can be informative when it comes to detecting changes in tertiary structure caused by, for example, the binding of agonists. The intrinsic fluorescence of tryptophans residing in a non-polar environment may be quenched or shifted in wavelength by direct interaction with a ligand or due to induced conformational changes exposing the tryptophan to a different milieu (38). In AgTRPA1, there are 13 tryptophan residues, of which eight are retained in Δ1–776 AgTRPA1 (Fig. 3*A*). An alignment with the sequence of the recently reported structure of hTRPA1 (39) reveals that five of the corresponding amino acid residues are resolved in the structure and that tryptophans 915, 926, and 1108 are likely to be located on the surface of the protein, interacting with detergent in the micelle or the aqueous phase (Fig. 3*B*). Two conserved tryptophans, corresponding to Trp-779 and Trp-950 in AgTRPA1, are buried in the structure: a classification of these tryptophans in the structure of hTRPA1 using PFAST (Protein Fluorescence and Structure Toolkit (40)) suggests that the former is located in a fairly polar environment (class III, $p = 0.87$), whereas the latter is packed into more hydrophobic milieu (class S ($p = 0.55$) or class I ($p = 0.45$)). The conserved amino acid residues within 5 Å of the two tryptophan indole rings (Fig. 4) support a similar polar and hydrophobic setting in AgTRPA1 for Trp-779 and Trp-950, respectively. The expected emission maximum for a tryptophan of class III is between 346 and 350 nm, whereas the ranges for tryptophans belonging to classes S and I are blue-shifted to 321–325 and 330–333 nm (40). Concentration-response

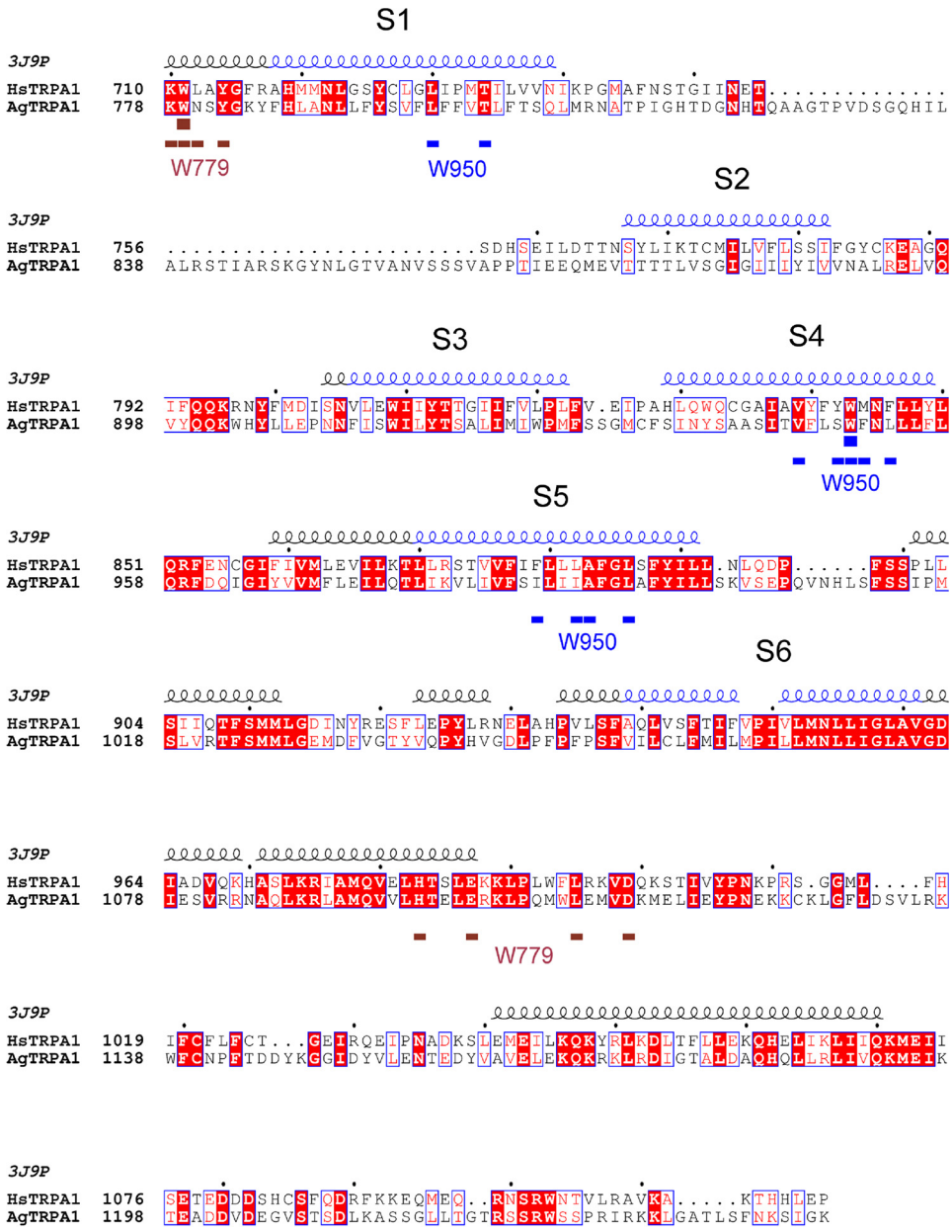

FIGURE 4. **Conservation of residues surrounding Trp-779 and Trp-950.** Alignment of hTRPA1 and AgTRPA1 omitting the N-terminal ARD. The secondary structure of hTRPA1 extracted from PDB entry 3J9P is displayed at the *top* with transmembrane helices S1–S6 *colored* in *blue*. Residues within 5 Å of the indole rings of two tryptophans in 3J9P corresponding to Trp-779 and Trp-950 of AgTRPA1 are indicated in *brown* and *blue*, respectively, *below* the alignment.

experiments show that both constructs have intrinsic tryptophan fluorescence with a maximum at 337 nm, which can be totally quenched by the agonist AITC without any associated shift of the maximum in the spectra (Fig. 5*A*). Although statistical analysis favors a model with different pEC_{50} values for AITC of the two constructs ($p < 0.005$), the corresponding EC_{50} values 256 and 444 μM, for AgTRPA1 and Δ1–776 AgTRPA1, respectively, differ less than 2-fold.

To investigate whether the quenching of tryptophan fluorescence also occurs at thermal activation of the protein, we monitored the tryptophan fluorescence as a function of temperature in the interval 25–48 °C (Fig. 5*B*). There is indeed a thermal quenching with a midpoint at 38.7 ± 1.0 and 41.1 ± 3.3 °C for AgTRPA1 and Δ1–776 AgTRPA1, respectively, and similar to the ligand-induced quenching, there is no associated shift of the wavelength for the maximal intensity. Notably, in contrast to AITC, the maximal quenching in the temperature range investigated does not totally abolish the fluorescence. Instead, the intensity at the highest temperature corresponds to about half of the non-quenched signal.

Chemical and Heat Activation of AgTRPA1—Several studies have shown that heterologously expressed AgTRPA1 is activated by electrophilic compounds and by heat and that the TRP channel pore blocker ruthenium red inhibits the activity evoked by such stimuli (12, 16, 17, 23, 24). In this study, we used AITC and, to a lesser extent, cinnamaldehyde to study electrophile activation of purified AgTRPA1 with and without its N-terminal ARD. As shown in patch-clamp voltage ramp recordings, both AgTRPA1 and Δ1–776 AgTRPA1 when inserted into planar lipid bilayers were activated by either AITC or cinnamalde-

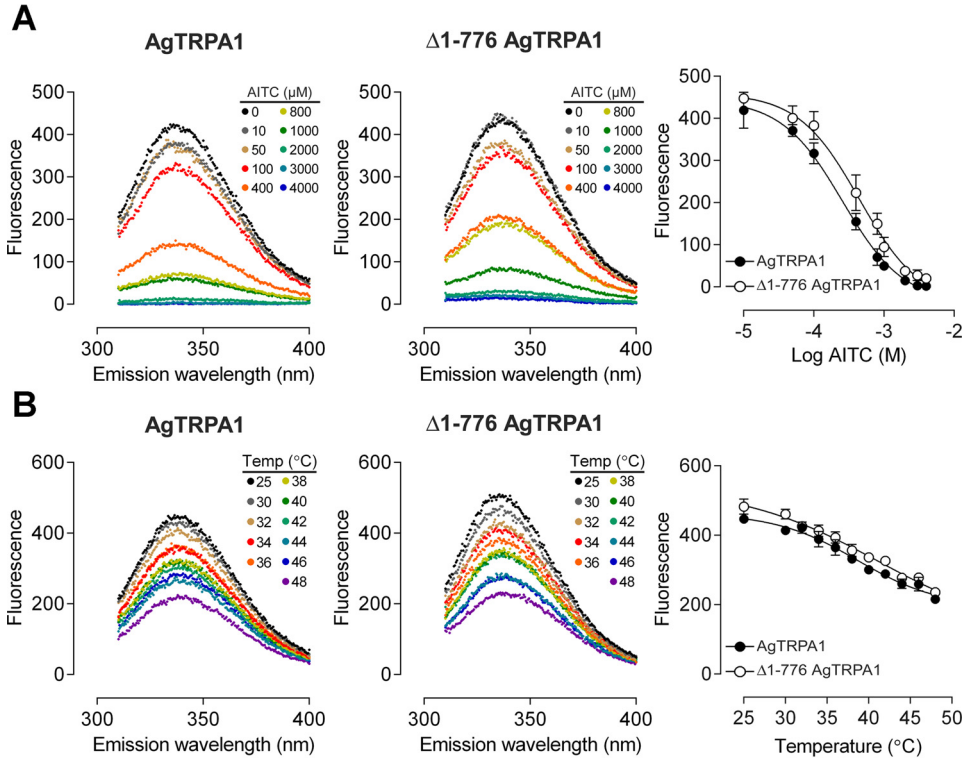

FIGURE 5. **Quenching of intrinsic tryptophan fluorescence.** *A*, binding of AITC quenches the tryptophan fluorescence emission intensity at 337 nm of AgTRPA1 and Δ1–776 AgTRPA1 in a concentration-dependent manner. The data were fitted to a sigmoidal concentration-response equation, and the EC_{50} was estimated to be 256 and 444 μM (3.591 ± 0.046 and 3.352 ± 0.056; average pEC_{50} ± S.E.; $n = 4$) for AgTRPA1 and Δ1–776 AgTRPA1, respectively. The null hypothesis with a common pEC_{50} value was rejected ($p < 0.005$). *B*, temperature-induced quenching of intrinsic tryptophan fluorescence of AgTRPA1 and Δ1–776 AgTRPA1. The midpoints are 38.7 ± 1.0 and 41.1 ± 3.3 °C (average ± S.E.; $n = 3$) for AgTRPA1 and Δ1–776 AgTRPA1, respectively. No shift is detected in the intrinsic fluorescence maximal intensity wavelength when AgTRPA1 or Δ1–776 AgTRPA1 is exposed to either AITC (*A*) or temperature (*B*).

hyde (each 100 μM) at negative and positive test potentials (Figs. 6–8). This concentration of AITC and cinnamaldehyde has been shown to evoke robust insect TRPA1 responses (12, 24). Importantly, the vehicle of AITC and cinnamaldehyde (1% ethanol) had no effect on AgTRPA1 and Δ1–776 AgTRPA1 (Figs. 6 and 7), and neither AITC nor cinnamaldehyde evokes currents in bilayers without protein (14). At a steady state test potential of +60 mV, we observed mainly one single-channel current level and occasionally a lower single-channel current level when using AITC as agonist. Analysis of the main single-channel current level showed higher single-channel mean conductance (G_s) and lower P_o values for Δ1–776 AgTRPA1 as compared with AgTRPA1 (Table 2). As shown for AgTRPA1, the AITC-induced activity was inhibited by ruthenium red at a concentration of 40 μM ($n = 4$; Fig. 6), which is within the concentration range that abolished both AITC and heat activation of heterologously expressed AgTRPA1 (12, 16, 23).

Heat responses of AgTRPA1 and Δ1–776 AgTRPA1 were observed in voltage ramp recordings (−100 to +100 mV in 2 s) and studied in detail at a single-channel level at a steady state test potential of +60 mV (Fig. 9). Both TRPA1 channels displayed intense channel activity at 30 °C and above (Fig. 9). No activity was shown in bilayers without AgTRPA1 and Δ1–776 AgTRPA1 ($n = 4$; not shown) (25). At 25 °C, sporadic activity of AgTRPA1, but not of Δ1–776 AgTRPA1, was recorded (Fig. 9). Using a simplified approach (41, 42), a Q_{10} value of 28 was calculated for AgTRPA1 using P_o values at 25 and 30 °C from three separate bilayer recordings. The analysis of G_s and P_o at a steady state test potential of +60 mV revealed differences between AgTRPA1 with and without its N-terminal ARD (Table 2). Thus, at 30 °C, the G_s for Δ1–776 AgTRPA1 was 39% of that for AgTRPA1 (Table 2). However, when the temperature was raised to 40 °C, the G_s for Δ1–776 AgTRPA1 increased by 72%, whereas the G_s for AgTRPA1 decreased by 46% (Table 2). Although not reaching statistical significance, raising the temperature from 30 to 40 °C increased the P_o by 45% for Δ1–776 AgTRPA1 (Table 2). As shown by continuous recordings, the heat responses were temperature-dependent in a reversible manner (Fig. 10).

Discussion

Studies of isolated proteins are crucial for elucidation of the molecular mechanisms responsible for activation of thermo- and chemoreceptors. Here we report on the heterologous expression and purification of functional full-length AgTRPA1 as well as the truncated Δ1–776 AgTRPA1, lacking the N-terminal ARD. The truncated version not only produced a higher yield than the full-length protein; it also formed a more stable tetramer under the conditions applied because most of the protein eluted in the tetrameric peak when size exclusion chromatography was applied. In contrast, almost half of the full-length AgTRPA1 was lost in dimeric fractions. The tetrameric structures suggest that the isolated proteins are correctly folded. This was confirmed by SRCD measurements generating characteristic spectra for α-helical proteins. Although the quaternary structure of Δ1–776 AgTRPA1 appeared more stable,

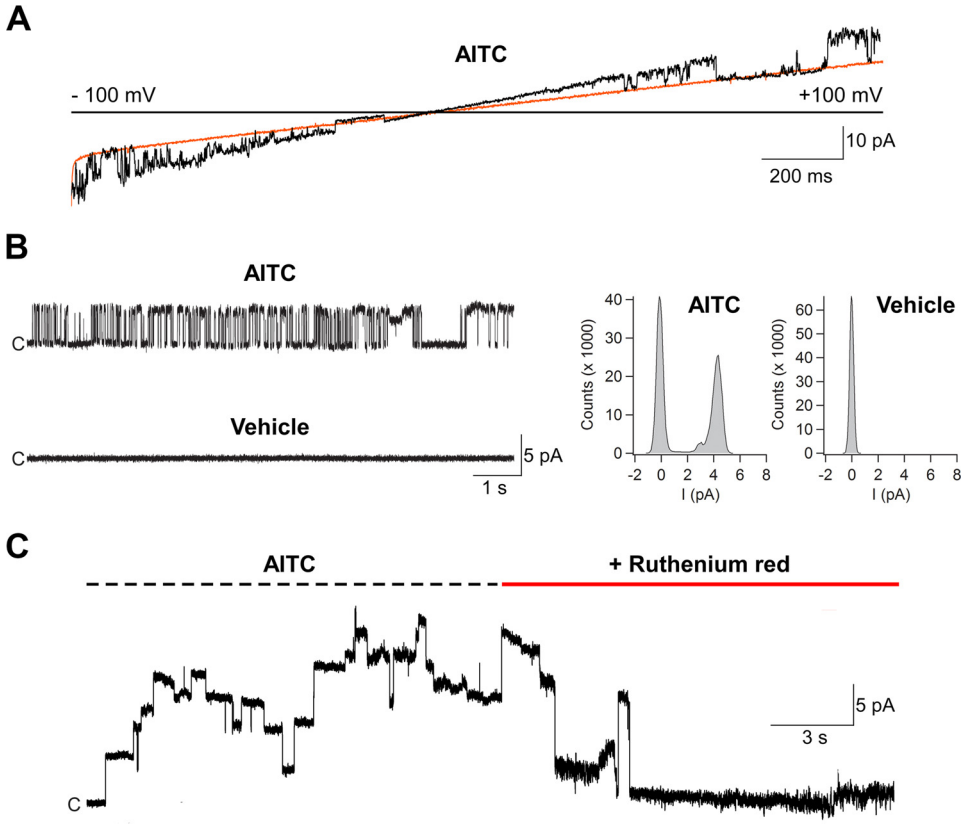

FIGURE 6. **The electrophilic compound AITC activates purified AgTRPA1.** *A*, as shown in experiments measuring ramp currents (−100 to +100 mV in 2 s), AgTRPA1 responded to AITC (100 μM) with inward and outward channel currents (*black trace*) at negative and positive test potentials, respectively. The *orange trace* shows baseline currents. *B*, at a steady state test potential of +60 mV, distinct single-channel openings were observed. The vehicle (1% ethanol) of AITC and cinnamaldehyde (Fig. 8) did not evoke activation of AgTRPA1. Shown are representative traces and corresponding amplitude histograms (see Table 2 for calculated single-channel G_s and P_o values). *C*, the non-selective TRP channel blocker ruthenium red (40 μM) abolished the activity of several AgTRPA1 channels. Purified AgTRPA1 was inserted into planar lipid bilayers, and channel currents were recorded with the patch-clamp technique in a symmetrical K^+ solution (*c*, closed channel state; *upward deflections*, open channel state).

there was more variability between samples at the lower temperatures of the thermal denaturation curve, as compared with the full-length construct. This might hint that the N-terminal ARD helps to stabilize the helical content at lower temperatures. However, overall, the thermal stabilities of the two constructs were very similar, and there appear to be some minor transitions between 25 and 45 °C in both constructs, although compelling evidence for common distinct transitions specifically coupled to the thermal activation of the channel is missing due to the variation between samples.

Tryptophan fluorescence might be quenched by a direct interaction with the ligand or may report on subtle conformation changes that are not detected by CD. Surprisingly, both constructs had a similar molar intrinsic fluorescence. Although a simple explanation would be that the five tryptophans in the N-terminal ARD do not contribute much to the fluorescence of AgTRPA1, there are other possibilities. Further studies of the fluorescence intensity decay might resolve the contributing residues.

The EC_{50} of fluorescence quenching is somewhat high compared with functional studies of activation of AgTRPA1 by AITC in CHO cells (70.7 ± 12.4 μM) (24). This may indicate that some low affinity binding sites that are required to bind AITC for complete quenching are not necessary for the activation of the protein by this agonist and that any conformational changes associated with activation of the channel are not sufficient to obtain complete quenching. This is in line with the partial quenching obtained by temperature. The full-length AgTRPA1 and the truncated construct exhibit similar temperature quenching curves, and it is interesting to note how well they follow each other between 40 and 46 °C with a common transition between 42 and 44 °C. Identification of tryptophans that contribute to the fluorescence may indicate where AITC binds and, more importantly, where structural changes take place. AITC is expected to bind to cysteines and lysines. In AgTRPA1, there are 65 lysines and 23 cysteines, but there are only 25 lysines and 4 cysteines in the truncated variant. Examination of the corresponding amino acid residues in the recently solved hTRPA1 structure (39) allows a crude evaluation of the environment where some of the tryptophans reside. From this structural analysis, Trp-950 appears as a promising candidate for some of the intrinsic fluorescence that is quenched by activation of the channel. It is situated in a hydrophobic pocket at the interface between S1 and S5 helices of neighboring subunits and may therefore report on conformational changes in the tetramer. This is supported by the fact that there are no lysines or cysteines in the close vicinity of Trp-950 that could act as binding sites. The changes in conformation reflected by quenching of fluorescence may report on the activation state of the channel and can potentially be used to inves-

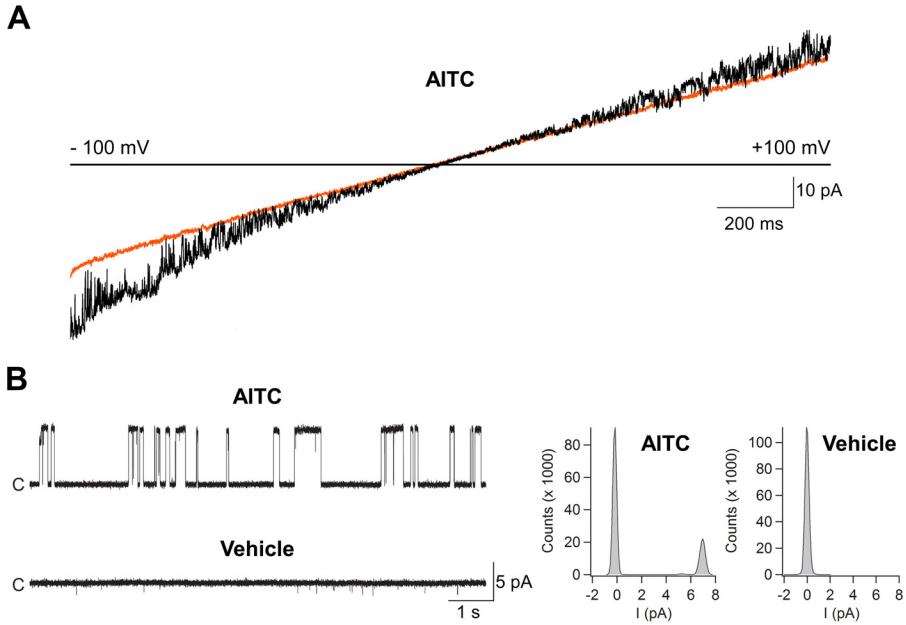

FIGURE 7. **The electrophilic compound AITC activates purified AgTRPA1 lacking its N-terminal ARD.** *A*, as shown in experiments measuring ramp currents (−100 to +100 mV in 2 s), AgTRPA1 without its N-terminal ARD (Δ1–766 AgTRPA1) responded to AITC (100 μM) with inward and outward channel currents (*black trace*) at negative and positive test potentials, respectively. The *orange trace* shows baseline currents. *B*, at a steady state test potential of +60 mV, distinct single-channel openings were observed. The vehicle (1% ethanol) of AITC and cinnamaldehyde (Fig. 8) did not evoke activation of Δ1–766 AgTRPA1. Shown are representative traces and corresponding amplitude histograms (see Table 2 for calculated single-channel G_s and P_o values). Purified Δ1–766 AgTRPA1 was inserted into planar lipid bilayers, and channel currents were recorded with the patch clamp technique in a symmetrical K^+ solution (*c*, closed channel state; *upward deflections*, open channel state).

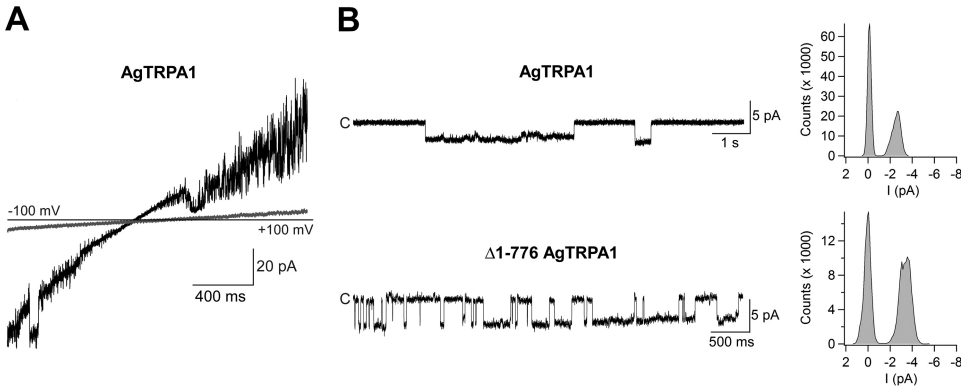

FIGURE 8. **The electrophilic compound cinnamaldehyde activates purified AgTRPA1 with and without its N-terminal ARD.** *A*, as shown in experiments measuring ramp currents (−100 to +100 mV in 2 s), AgTRPA1 responded to cinnamaldehyde (100 μM) with macroscopic inward and outward channel currents (*black trace*) at negative and positive test potentials, respectively. *Gray trace*, baseline currents. *B*, at a steady state test potential of −60 mV, distinct single-channel openings were observed for AgTRPA1 with and without its N-terminal ARD (Δ1–766 AgTRPA1). The vehicle (1% ethanol) of cinnamaldehyde did not evoke activation of AgTRPA1 or Δ1–766 AgTRPA1 (see Figs. 6 and 7). Shown are representative traces and corresponding amplitude histograms yielding single-channel conductances of 41 and 57 picosiemens for AgTRPA1 and Δ1–766 AgTRPA1, respectively. Purified AgTRPA1 and Δ1–766 AgTRPA1 were inserted into planar lipid bilayers, and channel currents were recorded with the patch-clamp technique in a symmetrical K^+ solution (*c*, closed channel state; *downward deflections*, open channel state).

tigate the mechanisms behind activation in a membrane-independent manner. We note that the complete integrated nexus, as recognized in the structure of hTRPA1, is missing in our truncated construct (39). This would indicate that neither activation by temperature nor AITC-mediated activation requires helix-turn-helix 1 or 2 of this intricate structure.

Our patch clamp studies provide evidence that the purified AgTRPA1 is a functional ion channel with and without its N-terminal ARD. We show for the first time, to our knowledge, that both thermo- and chemosensitivity of a non-mammalian TRPA1 are functionally relevant inherent channel properties. Using the purified AgTRPA1 without its N-terminal ARD allows us to conclude that TRPA1 polymodal sensory properties, which are proposed to be mediated by the N-terminal ARD domain (4), are also determined by channel structures outside the N-terminal ARD. A similar conclusion was reached regarding the intrinsically cold- and chemosensitive hTRPA1 (14). Although the possibility cannot be excluded that a truncation of AgTRPA1 may reveal hidden channel properties (5, 10), like exposure of new binding sites, studies of purified TRPA1 without its N-terminal ARD should be a valuable complementary strategy to identify the electrophile binding sites and temperature domains linked to TRPA1 channel gating.

TABLE 2
Single channel conductance and open probability values for AgTRPA1 and Δ1–776 AgTRPA1 activated by AITC and heat at a test potential of +60 mV

	AgTRPA1		Δ1–766 AgTRPA1		AgTRPA1		Δ1–766 AgTRPA1	
Stimuli	Conductance, mean ± S.E.	*n*	Conductance, mean ± S.E.	*n*	Open probability, mean ± S.E.	*n*	Open probability, mean ± S.E.	*n*
	pS		*pS*					
AITC (100 μM)	56 ± 6[a]	6	87 ± 3[a]	6	0.53 ± 0.06[b]	5	0.28 ± 0.05[b]	6
30 °C	74 ± 6[c,d]	3	29 ± 2[c,e]	4	0.45 ± 0.06	4	0.44 ± 0.04	5
40 °C	40 ± 4[d]	4	50 ± 3[e]	3	0.53 ± 0.06	4	0.64 ± 0.04	3

[a] $p < 0.01$; unpaired *t* test, two-tailed.
[b] $p < 0.05$; unpaired *t* test, two-tailed.
[c–e] $p < 0.0001$, one-way analysis of variance, multiple comparisons.

The AgTRPA1 exists as A and B isoforms, of which AgTRPA1(B) is extremely heat-sensitive (16). Corresponding isoform-dependent differences in heat properties have also been shown for *Drosophila* TRPA1, whereas the maximal response and sensitivity to the electrophilic compound *N*-methylmaleimide were not different (16), indicating that heat sensitivity may not always be evolutionarily gained at the expense of electrophile sensitivity (5, 26). Here, we have focused on AgTRPA1(A) because this isoform was originally reported as the heat-sensitive TRPA1 in *Anopheles gambiae* (17, 23). In agreement with these studies, we observed heat responses within the same temperature interval starting at 25 °C and reaching saturation at 30 °C for both G_s and P_o when compared with 40 °C. Although this very steep temperature-response interval (25–30 °C) did not allow us to perform a detailed thermodynamic analysis of Q_{10} and the thermal threshold for AgTRPA1(A) activation, our data suggest a Q_{10} of 28 based on P_o values obtained at 25 °C and 30 °C and a thermal threshold close to 25 °C, which is within the temperature activation range of this AgTRPA1 isoform when expressed in *Xenopus* oocytes (17, 23). However, a later study, also using the *Xenopus* oocyte expression system, determined a thermal threshold of 32 °C and a Q_{10} of 4 for AgTRPA1(A) (16). This discrepancy may perhaps be due to the AgTRPA1(A) basal activity observed below thermal threshold even at 15 °C (16). Furthermore, variation in channel expression levels and test potential are confounding factors in the thermodynamic analysis of TRP channels (42). Compared with AgTRPA1(B), AgTRPA1(A) has additional amino acids at the distal end of the N terminus reducing its heat sensitivity (16). However, without the N-terminal ARD, both isoforms of AgTRPA1 are identical and thus have the same thermo- and chemosensitive properties as described for Δ1–776 AgTRPA1 in the present study. Whether the N-terminal ARD of AgTRPA1(B) renders it more sensitive than AgTRPA1(A) to heat in our test system remains to be shown. Nevertheless, there is no doubt that the purified AgTRPA1(A) used in our study is a functional thermosensitive ion channel either intact or without its N-terminal ARD, because we could only observe heat responses in bilayers containing AgTRPA1 or Δ1–776 AgTRPA1. It has been suggested that the sensitivity of TRPA1 to electrophiles is species-dependent (4, 5). Indeed, at a single-channel current level, there are clear differences between the purified hTRPA1 and AgTRPA1 in such a way that we observed mainly one current level in AgTRPA1, whereas hTRPA1 displayed several current levels in response to AITC at 100 μM (14). The G_s, calculated for the main current level, was much lower for AgTRPA1 compared with hTRPA1 both in the presence and absence of the N-terminal ARD. Furthermore, without the N-terminal ARD, the P_o for AgTRPA1 was much smaller than that of hTRPA1 (14). Altogether, this may be related to differences in the number of cysteine residues, with hTRPA1 having 28 and AgTRPA1 23 cysteines, of which AgTRPA1 only has 4 cysteines compared with 9 for hTRPA1 outside the N-terminal ARD. Interestingly, the G_s and P_o of AgTRPA1(A), when exposed to heat and AITC, were different in the presence and absence of the N-terminal ARD, indicating that the temperature and chemosensitivity of AgTRPA1 is modulated by the N-terminal ARD, as has also been proposed for the purified hTRPA1 (14).

In conclusion, our study on the purified AgTRPA1 together with that on purified hTRPA1 (14) yield the important finding that heat and cold thermosensation as well as electrophile chemosensitivity of TRPA1 are also detected by channel structures and binding sites outside the N-terminal ARD. This TRPA1 thermo- and chemosensitive framework should help to identify the molecular mechanism behind temperature and ligand gating of TRPA1 as well as species-selective fine tuning chemicals of TRPA1 that can be used as analgesics and repellents.

Experimental Procedures

AgTRPA1 Overexpression and Purification—The coding sequence for AgTRPA1 (23) (accession number EU624401), referred to previously as isoform A (16), was inserted into the pPICZB vector in the SacII and NotI restriction sites, using forward primer TGCCGCGGCAAAATGTCTCCTACTCCGCTGTAC and reverse primer TTTTCCTTTTGCGGCCGCTTTGCCAATAGATTTGT (SacII and NotI sites underlined), resulting in a translational fusion with the plasmid-encoded C-terminal hexahistidine tag. An N-terminal truncated construct lacking the first 776 codons (*Δ1–776 AgTRPA1*) was also subcloned into the pPICZB vector between EcoRI and NotI restriction sites, using forward primer GCGGAATTCAAAATGTCTAAGTGGAACTCCTACGGC (EcoRI site underlined) and the same reverse primer as was used for the full-length construct. Both forward primers introduced an extra serine residue after the initiation methionine to optimize the translational initiation in *P. pastoris.*

The constructs were verified by DNA sequencing, and plasmids encoding the His-tagged AgTRPA1 (hereafter referred to as AgTRPA1) or the His-tagged Δ1–776 AgTRPA1 (hereafter referred to as Δ1–776 AgTRPA1) were electroporated into the methylotrophic *P. pastoris* strain X-33 (*Pichia* Expression Kit

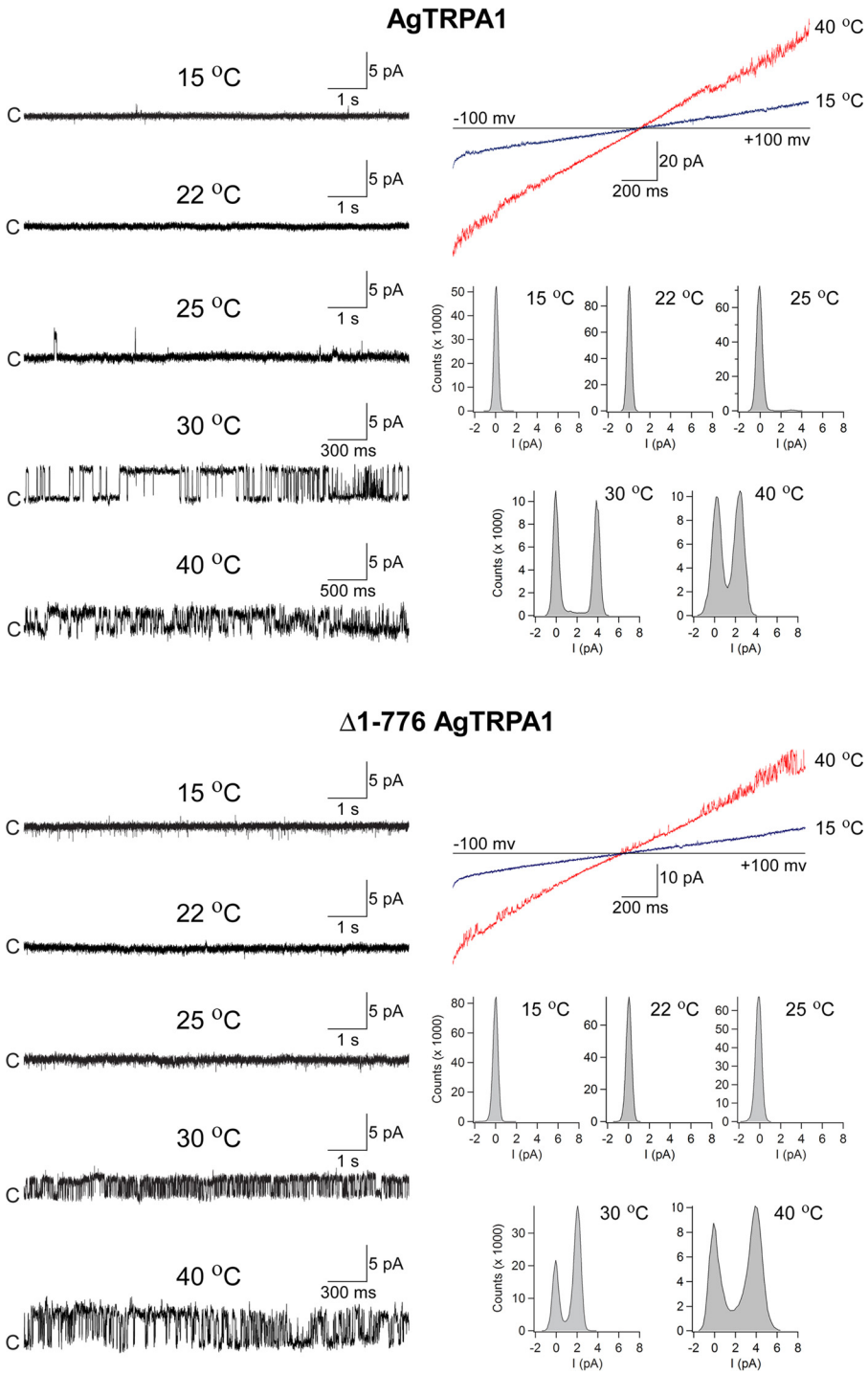

FIGURE 9. **Heat activates purified AgTRPA1 with and without its N-terminal ARD.** As shown in experiments measuring ramp currents (−100 to +100 mV in 2 s), AgTRPA1 and AgTRPA1 without its N-terminal ARD (Δ1–766 AgTRPA1) responded to increased temperatures with inward and outward channel currents (*red traces*) at negative and positive test potentials, respectively. At a steady state test potential of +60 mV, distinct single-channel openings were observed at 30 and 40 °C. Occasionally, channel opening appeared already at 25 °C for AgTRPA1, but never for Δ1–766 AgTRPA1 ($n = 3$). No activity was observed for AgTRPA1 and Δ1–766 AgTRPA1 at 15 and 22 °C ($n = 2$–3). Shown are representative traces and corresponding amplitude histograms (see Table 2 for calculated single-channel G_s and P_o values). Purified AgTRPA1 and Δ1–766 AgTRPA1 were inserted into proteoliposomes that were used to form planar lipid bilayers, and channel currents were recorded with the patch-clamp technique in a symmetrical K^+ solution (*c*, closed channel state; *upward deflections*, open channel state).

manual, Invitrogen). High gene copy clones were selected on zeocin as described previously (43), and the integrity of constructs was confirmed by PCR and subsequent agarose gel electrophoresis. Crude lysates of induced cultures were screened to identify high expression clones, using an anti-tetrahistidine antibody and Western blotting as described previously (43).

Large scale expression of AgTRPA1 and Δ1–776 AgTRPA1 was conducted in a 3-liter bench top fermenter (Belach Bioteknik). The cells obtained after expression in a fermenter

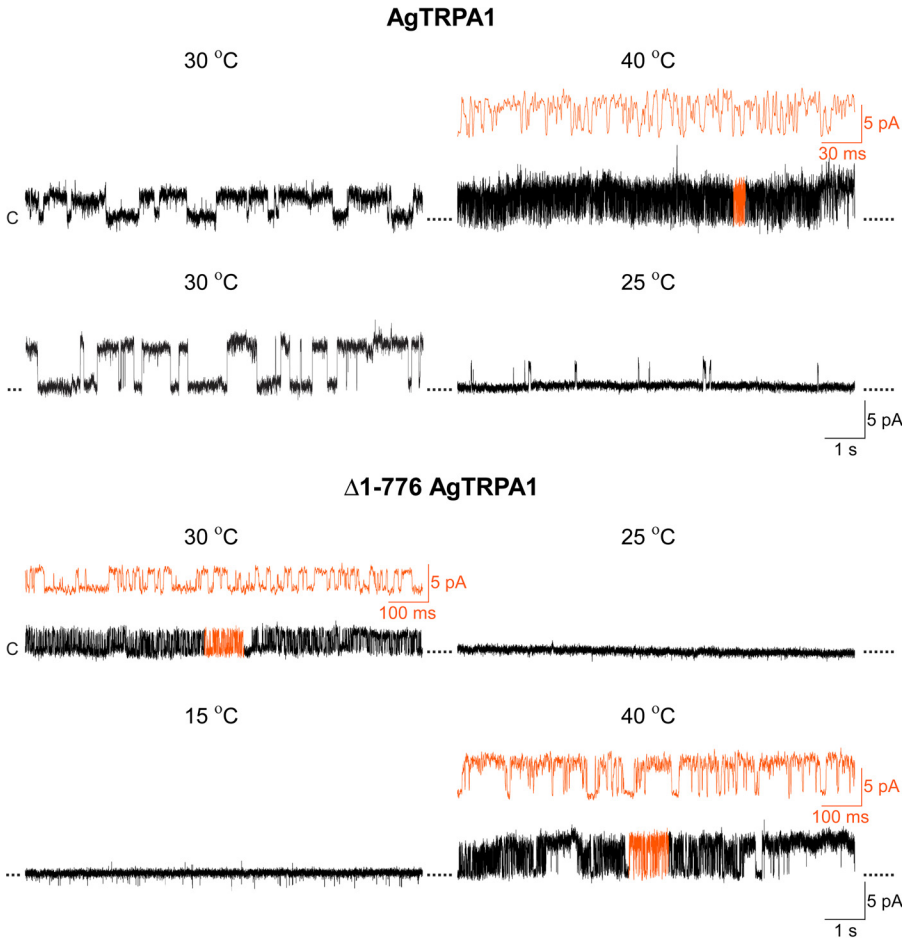

FIGURE 10. **Reversibility of AgTRPA1 heat responses.** The heat responses of AgTRPA1 with and without its N-terminal ARD (Δ1–766 AgTRPA1) were reversible when continuously exposed to different temperatures (30–35-min total recording time). Shown are representative recordings from 2–3 separate experiments. *Black traces* are shown at the same time scale (1 s), whereas *orange traces* show part of the recordings at a higher time resolution (30 and 100 ms). Purified AgTRPA1 (temperatures 30, 40, 30, and 25 °C) and Δ1–766 AgTRPA1 (temperatures 30, 25, 15, and 40 °C) were inserted into planar lipid bilayers, and channel currents were recorded with the patch clamp technique in a symmetrical K^+ solution at a test potential of +60 mV (*c*, closed channel state; *upward deflections*, open channel state).

were collected, and crude membrane was prepared as described elsewhere (44). Briefly, the cells were resuspended in ice-cold breaking buffer (50 mM NaH_2PO_4, 1 mM EDTA, 5% glycerol, 1 mM PMSF (MBL International Corp.), pH 7.4), and lysis was carried out using a bead beater (Biospec Products, Inc.). The cell lysate was centrifuged in the cold at 7,000 × *g* for 30 min to remove the cell debris, and the supernatant was centrifuged again at 100,000 × *g* for 2 h to pellet the crude membrane. The crude membranes were washed with urea and alkali to remove peripheral proteins (44).

The washed membranes were resuspended in buffer A (20 mM HEPES, 0.5 M NaCl, 10% glycerol, 2 mM β-mercaptoethanol, 1 mM PMSF, 100 μM leupeptin (Sigma-Aldrich), 10 μM pepstatin (Sigma-Aldrich), and 1% fos-choline-12 (FC-12; Anagrade, Anatrace), pH 7.8) at room temperature for 2 h to solubilize the AgTRPA1 and Δ1–776 AgTRPA1 protein. The soluble fraction was separated by ultracentrifugation at 100,000 × *g* for 30 min. The supernatant was loaded onto equilibrated Ni-NTA resin and incubated overnight at 4 °C with gentle agitation to allow binding of His-tagged proteins. The Ni-NTA resin was washed with buffer B (20 mM HEPES, 0.3 M NaCl, 10% glycerol, 2 mM β-mercaptoethanol, 1 mM PMSF, 100 μM leupeptin, 10 μM pepstatin, and 0.15% FC-12, pH 7.8) supplemented with 30 mM imidazole to remove loosely bound proteins, and the His-tagged proteins were eluted with 300 mM imidazole in buffer B. Eluted proteins were concentrated using a VIVASPIN concentrator with a 50 and a 100 kDa cut-off for Δ1–776 AgTRPA1 and AgTRPA1, respectively.

The proteins were further purified on a Hiload Superdex 200 16/60 gel filtration column (GE Healthcare) equilibrated with PBS buffer (10 mM potassium phosphate, 150 mM NaCl, pH 7.5) supplemented with 10% glycerol and 0.15% FC-12. The purity of AgTRPA1 and Δ1–776 AgTRPA1 was assessed by SDS-PAGE and Western blotting. The protein concentration was determined with a NanoDrop spectrophotometer using calculated extinction coefficients based on the amino acid composition (ProtParam, available from the ExPASy website). The extinction coefficients for AgTRPA1 and Δ1–776 AgTRPA1 in water measured at 280 nm were 121,475 and 69,580 M^{-1} cm^{-1}, respectively. Fractions of the tetramer peak (marked by an *asterisk* in Fig. 1*B*) corresponding to AgTRPA1 fractions 45–48 (equivalent to elution volume in ml) and to Δ1–776 AgTRPA1 fractions 48–52 in the presented chromatograms were collected for further functional and structural studies.

SDS-PAGE and Western Blotting—Protein samples were mixed with 6× sample loading buffer (125 mM Tris-HCl, pH 6.8, 20% glycerol, 4% SDS, 10% (v/v), 2.4 M β-mercaptoethanol, and 0.1% bromphenol blue) and incubated for 10 min at room temperature before separation on 12% SDS-PAGE. Protein bands were visualized by staining the gel with Coomassie Brilliant Blue R250.

Similarly, for Western blots, proteins were separated by SDS-PAGE and subsequently transferred to a PVDF membrane (Millipore). His-tagged AgTRPA1 and Δ1–776 AgTRPA1 were visualized by immunodetection. Briefly, a tetra-His antibody (Qiagen) was diluted 1:10,000 in TBS (50 mM Tris, 150 mM NaCl, pH 7.6) supplemented with 3% BSA and allowed to bind to the His-tagged protein on the PDVF membrane overnight at 4 °C. The secondary anti-mouse IgG antibody conjugated to horseradish peroxidase (GE Healthcare) was diluted 1:10,000 in TBS containing 10% nonfat milk powder and incubated with blots for 2 h at room temperature. The blots were washed with TBS containing 0.01% Tween 20 for 10 min three times and then developed by enhanced chemiluminescence (GE Healthcare).

SRCD—Far UV SRCD spectra of purified AgTRPA1 and Δ1–776 AgTRPA1, at a concentration of 0.6 and 1.3 mg/ml, respectively, in 10 mM potassium phosphate, 40 mM NaCl, 60 mM KF, 10% glycerol, and 0.15% FC-12, pH 7.5, were collected at beamline CD1 of the ASTRID2 storage ring at the University of Aarhus (Aarhus, Denmark). To monitor the temperature-dependent changes in secondary structure, spectra between 180 and 280 nm were collected at different temperatures (25–80 °C), allowing 5 min of equilibration time at each temperature. The temperature of the sample was set using Peltier elements regulated by a Eurotherm controller. All of the measurements were performed in a quartz cell (0.0102 cm path length). The buffer without protein was also measured to subtract the baseline from SRCD spectra (45). The subtracted SRCD (millidegrees) signals were normalized to the maximal values and plotted against the temperature to generate transition curves (46). To obtain midpoints, the data were fitted to a non-linear Boltzmann sigmoidal equation using GraphPad Prism version 6.00 (GraphPad Software, La Jolla, CA).

Tryptophan Fluorescence—Changes in emission of intrinsic tryptophan fluorescence upon binding of the electrophilic ligand, AITC, were monitored at ambient temperature (22 °C) using a PerkinElmer Life Sciences spectrofluorimeter. Briefly, the purified AgTRPA1 or Δ1–776 AgTRPA1 (0.6 μM) was pre-incubated with different concentrations of AITC (0–4,000 μM) for 15 min at room temperature. Excitation was done at 280 nm, and emission spectra were collected from 310 to 400 nm. The spectra for different concentrations of AITC without protein were also recorded in a similar manner to correct the baseline. The emission data at 337 nm were fitted to a sigmoidal dose-response equation using GraphPad Prism version 6.00 (GraphPad Software) to estimate pEC_{50} values. The extra-sum-of-squares F-test within GraphPad Prism was used to evaluate the null hypothesis of a shared pEC_{50} value for AgTRPA1 and Δ1–776 AgTRPA1. Temperature-dependent changes in fluorescence emission of AgTRPA1 were also examined from 25 to 48 °C, with a 2 °C interval. The temperature of the measuring cell was controlled by an external water bath connected to the fluorimeter. Three individual samples were incubated at each temperature point to determine the temperature-related change in fluorescence. Samples were first equilibrated for 5 min in the measuring cell at the set temperature before starting the fluorescence scanning.

A topology plot was generated with TeXtopo (47) via the web application Protter (48), based on manual alignments and the structure of hTRPA1 (PDB entry 3J9P). Structural pictures were rendered in PyMOL (49).

Preparation of Giant Unilamellar Vesicles—Giant unilamelleer vesicles (GUVs) were produced by the electroformation method, using a Vesicle Prep Pro Station (Nanion Technologies) (50, 51). Briefly, a lipid stock was prepared by mixing 10 mM 1,2-diphytanoyl-*sn*-glycero-3-phosphocholine and 1 mM cholesterol in trichloromethane. Approximately 20 μl of this solution was placed on the indium tin oxide (ITO)-coated glass slide and allowed to dry. After complete evaporation of trichloromethane, an O-ring was placed on the dry lipids. The ITO-coated glass surface is electrically conductive and serves as an electrode. To prevent conduction between two glass slides, 300 μl of 1 M sorbitol was added gently. The ITO-coated glass slides were assembled on the Vesicle Prep Pro Station (Nanion Technologies), orienting ITO-coated conductive surfaces toward each other. Vesicles were formed by electroswelling under the influence of an alternating electrical field for 2 h at 36 °C.

Reconstitution of Purified Proteins into Planar Lipid Bilayer or Giant Unilamellar Vesicles—Further, GUVs were used for making either planar lipid bilayers or proteoliposomes (50, 51). For formation of a planar lipid bilayer, 5 μl of GUV solution was pipetted onto the patch clamp chip (aperture of 1–2 μm), applying a negative pressure from −10 to −40 millibars to position vesicles over the aperture. The process of bilayer formation was controlled by Patch Control software (Nanion Technologies). Approximately 0.2 μl of AgTRPA1 or Δ1–776 AgTRPA1 protein micelle solution of concentration 50–100 μg/ml was added to preformed planar lipid bilayers (final concentration of protein, 0.15–0.2 μg/ml) in studies of the AITC responsiveness of the ion channels.

For preparation of proteoliposomes, the purified proteins were added to the GUV solution (final protein concentration of 2.5–10 μg/ml for AgTRPA1 and Δ1–776 AgTRPA1), and the mixture was incubated for 2 h at room temperature. Detergent was removed with polystyrene Biobeads SM2 (Bio-Rad), using 40 mg of beads/ml. After an initial incubation at room temperature for 2 h, the incubation was continued overnight at 4 °C, and Biobeads were subsequently removed by centrifugation. The proteoliposomes were applied onto the patch clamp chip to allow formation of planar lipid bilayers, as described above, and used in studies of heat activation of the ion channels.

Electrophysiological Recordings—A symmetrical K^+ solution of the following composition was used in all lipid bilayer recordings: 50 mM KCl, 10 mM NaCl, 60 mM KF, 20 mM EGTA, and 10 mM HEPES (adjusted to pH 7.2 with KOH). Signals were acquired with an EPC 10 amplifier (HEKA) and the data acquisition software PatchMaster (HEKA) at a sampling rate of 50 kHz. The recorded data were digitally filtered at 3 kHz. The patch clamp experiments were performed either at room tem-

perature or the stated temperatures. The Port-a-Patch was equipped with an external perfusion system (Nanion Technologies) and an SC-20 dual in-line solution heater/cooler connected to a temperature-controlled (CL-100) liquid cooling system (Warner Instruments) to control the temperature of the perfusion solution. Electrophysiological data were analyzed using Clampfit version 9 (Molecular Devices) and Igor Pro (Wave Metrics software). Data were filtered by a low pass Gaussian filter at 1,000 and 500 Hz for analyses and traces, respectively. The G_s value was obtained from Gaussian fit of all-points amplitude histograms based on a 0.1-picoampere separation. The single-channel mean P_o was calculated from time constant values, which were obtained from exponential standard fits of dwell time histograms.

The Q_{10} for P_o was obtained from the following equation (32, 41).

$$Q_{10} = \left(\frac{P_{O2}}{P_{O1}}\right)^{10/(T_2 - T_1)} \quad \text{(Eq. 1)}$$

Author Contributions—E. D. H., P. M. Z., and U. J. conceived and designed the study. P. M. Z. and U. J. directed the study. S. S., P. K., and U. J. planned, performed, and analyzed biochemical and biophysical experiments. L. M., E. D. H., and P. M. Z. contributed electrophysiology studies (L. M. and P. M. Z. planned, performed, and analyzed the experiments). S. S., P. M. Z., and U. J. drafted the manuscript. P. M. Z. and U. J. wrote the paper. All authors discussed the results and commented on the manuscript.

Acknowledgments—We thank Brita Sundén-Andersson and Adine Karlsson for technical assistance and Dr. Paul Garrity for providing a plasmid carrying the coding sequence for TRPA1(A) from A. gambiae. SRCD spectra were collected at ASTRID2 and sponsored by the CALIPSO program. We thank Dr. Nykola Jones and Dr. Søren Vrønning Hoffmann for providing time and assistance at ASTRID2.

References

1. Patapoutian, A., Tate, S., and Woolf, C. J. (2009) Transient receptor potential channels: targeting pain at the source. *Nat. Rev. Drug Discov.* **8,** 55–68
2. Nilius, B., and Owsianik, G. (2011) The transient receptor potential family of ion channels. *Genome Biol.* **12,** 218
3. Holzer, P. (2011) Transient receptor potential (TRP) channels as drug targets for diseases of the digestive system. *Pharmacol. Ther.* **131,** 142–170
4. Julius, D. (2013) TRP channels and pain. *Annu. Rev. Cell Dev. Biol.* **29,** 355–384
5. Laursen, W. J., Anderson, E. O., Hoffstaetter, L. J., Bagriantsev, S. N., and Gracheva, E. O. (2015) Species-specific temperature sensitivity of TRPA1. *Temperature* **2,** 214–226
6. Bautista, D. M., Movahed, P., Hinman, A., Axelsson, H. E., Sterner, O., Högestätt, E. D., Julius, D., Jordt, S. E., and Zygmunt, P. M. (2005) Pungent products from garlic activate the sensory ion channel TRPA1. *Proc. Natl. Acad. Sci. U.S.A.* **102,** 12248–12252
7. Jordt, S. E., Bautista, D. M., Chuang, H. H., McKemy, D. D., Zygmunt, P. M., Högestätt, E. D., Meng, I. D., and Julius, D. (2004) Mustard oils and cannabinoids excite sensory nerve fibres through the TRP channel ANKTM1. *Nature* **427,** 260–265
8. Bandell, M., Story, G. M., Hwang, S. W., Viswanath, V., Eid, S. R., Petrus, M. J., Earley, T. J., and Patapoutian, A. (2004) Noxious cold ion channel TRPA1 is activated by pungent compounds and bradykinin. *Neuron* **41,** 849–857
9. Macpherson, L. J., Geierstanger, B. H., Viswanath, V., Bandell, M., Eid, S. R., Hwang, S., and Patapoutian, A. (2005) The pungency of garlic: activation of TRPA1 and TRPV1 in response to allicin. *Curr. Biol.* **15,** 929–934
10. Zygmunt, P. M., and Högestätt, E. D. (2014) TRPA1. *Handb. Exp. Pharmacol.* **222,** 583–630
11. Panzano, V. C., Kang, K., and Garrity, P. A. (2010) Infrared snake eyes: TRPA1 and the thermal sensitivity of the snake pit organ. *Sci. Signal.* **3,** pe22
12. Kang, K., Pulver, S. R., Panzano, V. C., Chang, E. C., Griffith, L. C., Theobald, D. L., and Garrity, P. A. (2010) Analysis of *Drosophila* TRPA1 reveals an ancient origin for human chemical nociception. *Nature* **464,** 597–600
13. Story, G. M., Peier, A. M., Reeve, A. J., Eid, S. R., Mosbacher, J., Hricik, T. R., Earley, T. J., Hergarden, A. C., Andersson, D. A., Hwang, S. W., McIntyre, P., Jegla, T., Bevan, S., and Patapoutian, A. (2003) ANKTM1, a TRP-like channel expressed in nociceptive neurons, is activated by cold temperatures. *Cell* **112,** 819–829
14. Moparthi, L., Survery, S., Kreir, M., Simonsen, C., Kjellbom, P., Högestatt, E. D., Johanson, U., and Zygmunt, P. M. (2014) Human TRPA1 is intrinsically cold- and chemosensitive with and without its N-terminal ankyrin repeat domain. *Proc. Natl. Acad. Sci. U.S.A.* **111,** 16901–16906
15. Gracheva, E. O., Ingolia, N. T., Kelly, Y. M., Cordero-Morales, J. F., Hollopeter, G., Chesler, A. T., Sánchez, E. E., Perez, J. C., Weissman, J. S., and Julius, D. (2010) Molecular basis of infrared detection by snakes. *Nature* **464,** 1006–1011
16. Kang, K., Panzano, V. C., Chang, E. C., Ni, L., Dainis, A. M., Jenkins, A. M., Regna, K., Muskavitch, M. A., and Garrity, P. A. (2011) Modulation of TRPA1 thermal sensitivity enables sensory discrimination in *Drosophila*. *Nature* **481,** 76–80
17. Wang, G., Qiu, Y. T., Lu, T., Kwon, H. W., Pitts, R. J., Van Loon, J. J., Takken, W., and Zwiebel, L. J. (2009) *Anopheles gambiae* TRPA1 is a heat-activated channel expressed in thermosensitive sensilla of female antennae. *Eur. J. Neurosci.* **30,** 967–974
18. Wang, H., Schupp, M., Zurborg, S., and Heppenstall, P. A. (2013) Residues in the pore region of *Drosophila* transient receptor potential A1 dictate sensitivity to thermal stimuli. *J. Physiol.* **591,** 185–201
19. Viswanath, V., Story, G. M., Peier, A. M., Petrus, M. J., Lee, V. M., Hwang, S. W., Patapoutian, A., and Jegla, T. (2003) Opposite thermosensor in fruitfly and mouse. *Nature* **423,** 822–823
20. Karashima, Y., Talavera, K., Everaerts, W., Janssens, A., Kwan, K. Y., Vennekens, R., Nilius, B., and Voets, T. (2009) TRPA1 acts as a cold sensor *in vitro* and *in vivo*. *Proc. Natl. Acad. Sci. U.S.A.* **106,** 1273–1278
21. Sawada, Y., Hosokawa, H., Hori, A., Matsumura, K., and Kobayashi, S. (2007) Cold sensitivity of recombinant TRPA1 channels. *Brain Res.* **1160,** 39–46
22. Kremeyer, B., Lopera, F., Cox, J. J., Momin, A., Rugiero, F., Marsh, S., Woods, C. G., Jones, N. G., Paterson, K. J., Fricker, F. R., Villegas, A., Acosta, N., Pineda-Trujillo, N. G., Ramírez, J. D., Zea, J., *et al.* (2010) A gain-of-function mutation in TRPA1 causes familial episodic pain syndrome. *Neuron* **66,** 671–680
23. Hamada, F. N., Rosenzweig, M., Kang, K., Pulver, S. R., Ghezzi, A., Jegla, T. J., and Garrity, P. A. (2008) An internal thermal sensor controlling temperature preference in *Drosophila*. *Nature* **454,** 217–220
24. Xiao, B., Dubin, A. E., Bursulaya, B., Viswanath, V., Jegla, T. J., and Patapoutian, A. (2008) Identification of transmembrane domain 5 as a critical molecular determinant of menthol sensitivity in mammalian TRPA1 channels. *J. Neurosci.* **28,** 9640–9651
25. Moparthi, L., Kichko, T. I., Eberhardt, M., Högestätt, E. D., Kjellbom, P., Johanson, U., Reeh, P. W., Leffler, A., Filipovic, M. R., and Zygmunt, P. M. (2016) Human TRPA1 is a heat sensor displaying intrinsic U-shaped thermosensitivity. *Sci. Rep.* **6,** 28763
26. Cordero-Morales, J. F., Gracheva, E. O., and Julius, D. (2011) Cytoplasmic ankyrin repeats of transient receptor potential A1 (TRPA1) dictate sensitivity to thermal and chemical stimuli. *Proc. Natl. Acad. Sci. U.S.A.* **108,** E1184–E1191
27. Zhong, L., Bellemer, A., Yan, H., Ken, H., Jessica, R., Hwang, R. Y., Pitt, G. S., and Tracey, W. D. (2012) Thermosensory and nonthermosensory

isoforms of *Drosophila* melanogaster TRPA1 reveal heat-sensor domains of a thermoTRP channel. *Cell Rep.* **1,** 43–55
28. Hinman, A., Chuang, H. H., Bautista, D. M., and Julius, D. (2006) TRP channel activation by reversible covalent modification. *Proc. Natl. Acad. Sci. U.S.A.* **103,** 19564–19568
29. Macpherson, L. J., Dubin, A. E., Evans, M. J., Marr, F., Schultz, P. G., Cravatt, B. F., and Patapoutian, A. (2007) Noxious compounds activate TRPA1 ion channels through covalent modification of cysteines. *Nature* **445,** 541–545
30. Jabba, S., Goyal, R., Sosa-Pagán, J. O., Moldenhauer, H., Wu, J., Kalmeta, B., Bandell, M., Latorre, R., Patapoutian, A., and Grandl, J. (2014) Directionality of temperature activation in mouse TRPA1 ion channel can be inverted by single-point mutations in ankyrin repeat six. *Neuron* **82,** 1017–1031
31. Clapham, D. E., and Miller, C. (2011) A thermodynamic framework for understanding temperature sensing by transient receptor potential (TRP) channels. *Proc. Natl. Acad. Sci. U.S.A.* **108,** 19492–19497
32. Voets, T. (2012) Quantifying and modeling the temperature-dependent gating of TRP channels. *Rev. Physiol. Biochem. Pharmacol.* **162,** 91–119
33. Baez, D., Raddatz, N., Ferreira, G., Gonzalez, C., and Latorre, R. (2014) Gating of thermally activated channels. *Curr. Top. Membr.* **74,** 51–87
34. Hilton, J. K., Rath, P., Helsell, C. V., Beckstein, O., and Van Horn, W. D. (2015) Understanding thermosensitive transient receptor potential channels as versatile polymodal cellular sensors. *Biochemistry* **54,** 2401–2413
35. Liu, C., and Zwiebel, L. J. (2013) Molecular characterization of larval peripheral thermosensory responses of the malaria vector mosquito *Anopheles gambiae*. *PLoS One* **8,** e72595
36. Törnroth-Horsefield, S., Wang, Y., Hedfalk, K., Johanson, U., Karlsson, M., Tajkhorshid, E., Neutze, R., and Kjellbom, P. (2006) Structural mechanism of plant aquaporin gating. *Nature* **439,** 688–694
37. Horsefield, R., Nordén, K., Fellert, M., Backmark, A., Törnroth-Horsefield, S., Terwisscha van Scheltinga, A. C., Kvassman, J., Kjellbom, P., Johanson, U., and Neutze, R. (2008) High-resolution X-ray structure of human aquaporin 5. *Proc. Natl. Acad. Sci. U.S.A.* **105,** 13327–13332
38. Lakowicz, J. R. (2006) Principles of Fluorescence Spectroscopy. Springer, New York
39. Paulsen, C. E., Armache, J. P., Gao, Y., Cheng, Y., and Julius, D. (2015) Structure of the TRPA1 ion channel suggests regulatory mechanisms. *Nature* **520,** 511–517
40. Shen, C., Menon, R., Das, D., Bansal, N., Nahar, N., Guduru, N., Jaegle, S., Peckham, J., and Reshetnyak, Y. K. (2008) The protein fluorescence and structural toolkit: database and programs for the analysis of protein fluorescence and structural data. *Proteins* **71,** 1744–1754
41. Latorre, R., Vargas, G., Orta, G., and Brauchi, S. (2007) Voltage and temperature gating of thermoTRP channels. in *TRP Ion Channel Function in Sensory Transduction and Cellular Signaling Cascades* (Liedtke, W. B., and Heller, S. eds) CRC Pres, Boca Raton, FL
42. Vriens, J., Nilius, B., and Voets, T. (2014) Peripheral thermosensation in mammals. *Nat. Rev. Neurosci.* **15,** 573–589
43. Nordén, K., Agemark, M., Danielson, J. Å., Alexandersson, E., Kjellbom, P., and Johanson, U. (2011) Increasing gene dosage greatly enhances recombinant expression of aquaporins in *Pichia pastoris*. *BMC Biotechnol.* **11,** 47
44. Karlsson, M., Fotiadis, D., Sjövall, S., Johansson, I., Hedfalk, K., Engel, A., and Kjellbom, P. (2003) Reconstitution of water channel function of an aquaporin overexpressed and purified from *Pichia pastoris*. *FEBS Lett.* **537,** 68–72
45. Whitmore, L., and Wallace, B. A. (2004) DICHROWEB, an online server for protein secondary structure analyses from circular dichroism spectroscopic data. *Nucleic Acids Res.* **32,** W668–W673
46. Lees, J. G., Smith, B. R., Wien, F., Miles, A. J., and Wallace, B. A. (2004) CDtool: an integrated software package for circular dichroism spectroscopic data processing, analysis, and archiving. *Anal. Biochem.* **332,** 285–289
47. Beitz, E. (2000) T(E)Xtopo: shaded membrane protein topology plots in LAT(E)X2epsilon. *Bioinformatics* **16,** 1050–1051
48. Omasits, U., Ahrens, C. H., Müller, S., and Wollscheid, B. (2014) Protter: interactive protein feature visualization and integration with experimental proteomic data. *Bioinformatics* **30,** 884–886
49. DeLano, W. L. (2010) *The PyMOL Molecular Graphics System*, version 1.5.0.4, Schroedinger, LLC, New York
50. Gassmann, O., Kreir, M., Ambrosi, C., Pranskevich, J., Oshima, A., Röling, C., Sosinsky, G., Fertig, N., and Steinem, C. (2009) The M34A mutant of Connexin26 reveals active conductance states in pore-suspending membranes. *J. Struct. Biol.* **168,** 168–176
51. Kreir, M., Farre, C., Beckler, M., George, M., and Fertig, N. (2008) Rapid screening of membrane protein activity: electrophysiological analysis of OmpF reconstituted in proteoliposomes. *Lab Chip* **8,** 587–595